Electronic properties of germanene on pristine and defective MoS₂: A first-principles study

Pengfei Lv[1], José Ángel Silva-Guillén[2,1,*], Alexander N. Rudenko[3,1] and Shengjun Yuan[1,†]

[1]*School of Physics and Technology, Wuhan University, Wuhan 430072, People's Republic of China*
[2]*Fundación IMDEA Nanociencia, C/Faraday 9, Campus Cantoblanco, 28409 Madrid, Spain*
[3]*Radboud University, Institute for Molecules and Materials, 6525AJ Nijmegen, The Netherlands*

The synthesis of germanene on semiconducting substrates such as MoS₂ has revealed that it exhibits a V-shaped density of states around the Fermi level, indicating the presence of Dirac electrons. Further experiments demonstrated that charge inhomogeneities of germanene on MoS₂ appear as *n*- and *p*-type doped regions, the origin of which is not well understood. In this paper, by means of density functional theory calculations, we study germanene deposited on MoS₂ considering various defect types and a variety of stacking configurations. We find that some native defects typical to MoS₂ samples lead to the charge transfer between germanene and MoS₂. Unlike vacancies and antisite defects, substitution of molybdenum by group IV-V and VII transition metal atoms does not lead to any midgap states, and appears as a plausible explanation for the experimentally observed charge puddles. Our results shed light on the mechanism of breaking the charge neutrality in Dirac materials without altering their electronic properties, which could be important for the realization of lateral *p-n* junctions based on two-dimensional materials.

I. INTRODUCTION

Germanene is an ideal two-dimensional (2D) Dirac material which has been extensively studied in recent years [1,2]. One of its most exciting features is that it presents a spin-orbit gap of around 24 meV [3], making it a good candidate to exhibit quantum spin Hall effect at temperatures that can be easily attained experimentally. In the last few years, several groups have focused their efforts on synthesizing germanene and its characterization [4–11]. However, in most of these experiments, germanene is grown on a metallic substrate, which has the main disadvantage of the coupling of the electronic states of germanene with those of the substrate around the Fermi level [2]. In order to avoid this issue and be able to characterize the electronic properties of germanene experimentally, a band gap material such as MoS₂ or hexagonal boron nitride should be used. Recently, the successful synthesis of germanene on MoS₂ by Zhang *et al.* [12] revealed that the electronic structure of germanene on MoS₂ substrates shows a prominent V-shaped density of states (DOS) around the Fermi level, which is one of the most distinct features of 2D Dirac materials.

Although the agreement between first-principles calculations and scanning tunneling spectroscopy for germanene on MoS₂ is good [12], theoretical calculations predict that the Fermi level is shifted from the Dirac point giving rise to finite DOS at the neutrality point. One possible explanation for this shift is the presence of impurities with an acceptor character in the germanene layer emerging during the growth process [12].

However, in a later work, it was found that there is no indication of defects or impurities of this type [13]. Furthermore, by analyzing the differential conductivity (*dI/dV*) spectra and using a Dirac-point mapping technique it was found that the germanene sample actually presents charge puddles, with *n*- and *p*-type doped regions. The origin of these electron and hole puddles can be likely attributed to defects and impurities in the MoS₂ layers.

Typically MoS₂ samples are mainly fabricated either by exfoliating natural geological samples or by chemical vapor deposition (CVD) [14–16]. Even if the the experimental samples are very clean, avoiding the formation of defects is challenging [17]. Although there have been previous studies on the effect of defects on the electronic properties of MoS₂ [17–21], the impact of defects on the electronic properties of the material that is deposited on top, specifically germanene, is unclear.

In this paper, we perform a comprehensive study of the electronic properties of germanene on MoS₂ using density functional theory (DFT). We focus on the role of defects in MoS₂ in the electronic properties of germanene. We find that, in experimental samples, germanene lies on top of MoS₂ without suffering any kind of alteration to its structure. Furthermore, we realize that substitutional atoms can explain the different reported *n*- and *p*-doped regions found on experimental samples.

This paper is organized as follows. In Sec. II, we describe the computational methods used to perform our calculations. Our results and discussion are presented in Sec. III, which is divided into two main parts. In the first part (Sec. III A), we analyze the effect of strain and the substrate on the electronic properties of germanene. In the second part (Sec. III B), we systematically study the role of realistic defects in MoS₂ on

*josilgui@gmail.com
†s.yuan@whu.edu.cn

the electronic properties of supported germanene. In Sec. IV, we conclude the paper with a short summary.

II. COMPUTATIONAL METHODS

All the calculations were performed using density functional theory [22] as implemented in the SIESTA code [23]. The wave functions have been expanded in a double-ζ basis set including polarization functions. We have used the Perdew-Burke-Ernzerhof parametrization [24] of the generalized gradient approximation [25] to describe the exchange-correlation effects, and the atomic core electron interactions were represented by norm-conserving Troullier-Martin pseudopotentials [26]. Van der Waals corrections were also taken into consideration using the Grimme parametrization [27]. A 20-Å-thick vacuum slab was added in the out-of-plane direction to avoid interactions between neighboring cells due to periodic boundary conditions. A real-space integration grid of 400 Ry was set. In order to converge the ground state charge density, the **k** space was sampled using the Monkhorst-Pack scheme [28] with a $(7 \times 7 \times 1)$ grid. The structure was relaxed with a tolerance of 0.05 eV/Å for the forces acting on the Ge atoms while keeping the MoS$_2$ layer fixed. For the structures with defects, we let the MoS$_2$ layer relax as well to correctly describe the defective structure. For the DOS calculations, the Brillouin zone was sampled using a $(71 \times 71 \times 1)$ **k**-point mesh. It is also worth mentioning that the main results remain the same when spin-orbit coupling [29] is included.

We have also calculated the formation energies of the different defects that can occur in the system. To do so, we define the formation energy as [30]

$$E^f[X] = E_{\text{tot}}[X] - E_{\text{tot}}[\text{pri}] - \sum_i n_i \mu_i, \qquad (1)$$

where $E_{\text{tot}}[X]$ and $E_{\text{tot}}[\text{pri}]$ are the total energies of the supercell with X impurities and the pristine system without any defects, respectively. n_i is the number of atoms of type i that have been added to ($n_i > 0$) or removed from ($n_i < 0$) in the defective system, and μ_i are the corresponding chemical potentials of these elements.

To calculate the chemical potential we use

$$\mu_{\text{Mo}} = \frac{1}{N} E_{\text{tot}}[\text{Mo}], \qquad (2)$$

$$2\mu_S + \mu_{\text{Mo}} = \mu_{\text{MoS}_2} = E_{\text{tot}}[\text{MoS}_2], \qquad (3)$$

where μ_{Mo} is the chemical potential of Mo, obtained from the bcc molybdenum structure, and μ_S is the chemical potential of S, which is calculated using μ_{Mo} and the total energy of a MoS$_2$ monolayer ($E_{\text{tot}}[\text{MoS}_2]$) [31]. The chemical potentials of the substitutional atoms such as Re, Zr, and Nb are determined by the total energy of their monolayer dichalcogenide form:

$$2\mu_S + \mu_X = \mu_{X\text{S}_2} = E_{\text{tot}}[X\text{S}_2]. \qquad (4)$$

On the other hand, we calculate the chemical potential of P and Cl using the energies of their bulk phase:

$$\mu_X = \mu_X[X, \text{bulk}] = \frac{1}{N} E_{\text{tot}}[X, \text{bulk}]. \qquad (5)$$

III. RESULTS AND DISCUSSION

A. Electronic properties of germanene on top of pristine MoS$_2$

As stated in the Introduction, the experimental results show that the Dirac cone sits exactly at the Fermi level [12,13]. Although the theoretical results match qualitatively with the experimental spectra, there is a mismatch of the Fermi level between the experimental and theoretical results [12]. It is well known that strain affects the electronic properties of germanene [32], therefore, in order to fully understand the disagreement between the theoretical results and the experimental measurements, we first studied if the MoS$_2$ substrate could affect the electronic properties of germanene when deposited on top of it [32,33]. To correctly calculate the strain applied to germanene we first need to calculate the lattice parameter for the unit cell of pristine germanene. We find that the optimized value is 4.09 Å, which is in agreement with previous calculations [34,35]. In order to study theoretically the electronic properties of germanene on a substrate we need to take into account the fact that germanene and MoS$_2$ do not have the same lattice constant and we have to impose the commensurability of the structure in order to perform the calculations. A typical approach used is to simply align the sample layer and the substrate and generate two different supercells to minimize the mismatch between the lattice parameter of both materials. This approach is ideal to study the effect of strain on the electronic properties of germanene when deposited on MoS$_2$.

As in previous studies, in our calculations we can also see that the strain applied to germanene has a great influence on the electronic properties of the supercells when placing it on top of MoS$_2$. As a first approach, we generate a supercell using the experimental value for the lattice constant of germanene, 3.82 Å [about -7% compression strain relative to that of freestanding germanene, see Fig. S1 of the Supplemental Material (SM) [37]]. We find that the DOS results are in line with previous DFT calculations [12], i.e., the position of the Dirac cone shifts ~ 0.3 eV towards lower energies (see SM [37] Fig. S1b for the total and partial DOS). To further investigate the strain effects of germanene on MoS$_2$, we also construct supercells with different sizes which allows us to have values for the applied strain to germanene around -5%. As we can see from Fig. 1, the position of the Dirac cone is very sensitive to strain and, as we reduce slightly the compressive strain applied, the energy position of the Dirac cone shifts towards higher energies. Therefore, most likely, in the experiment the crystalline structure of germanene does not suffer any alteration when deposited on top of MoS$_2$ and, in order to reproduce correctly these results, we need to generate a supercell using the optimized lattice constant of germanene. Unfortunately, in our case, we find that in order to achieve a small mismatch using two aligned layers as described above, a large supercell has to be computed.

To tackle the problem of large supercells, we can introduce the rotation between each layer as a degree of freedom. Importantly, this allows us to have lower values of strain applied to each of the materials while keeping the sizes within a reasonable number of atoms. We find that for a twist angle of 14.5° the mismatch between germanene is approximately -0.06%. The corresponding supercell is made of a $(\sqrt{19} \times \sqrt{19})$ layer
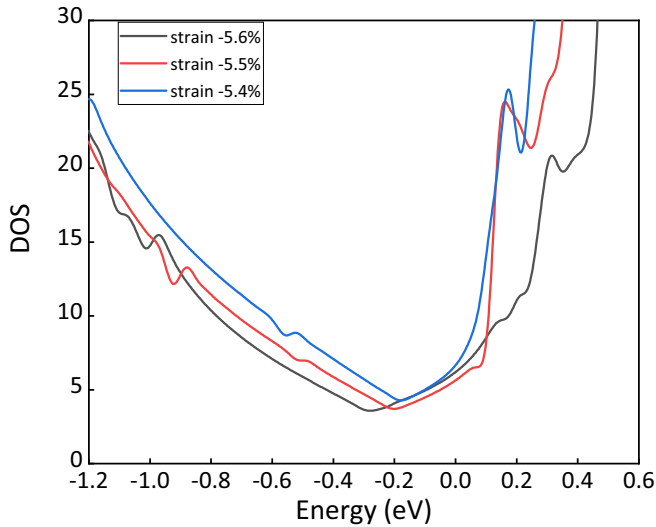
FIG. 1. Calculated DOS of three supercells with different compression strain of germanene. The position of the Dirac cone is sensitive to the biaxial compression strain of germanene. The three supercells consist of $(\sqrt{19} \times \sqrt{19})$ germanene/$(\sqrt{28} \times \sqrt{28})$ MoS$_2$, $(\sqrt{21} \times \sqrt{21})$ germanene/$(\sqrt{31} \times \sqrt{31})$ MoS$_2$, and (5×5) germanene/$(\sqrt{37} \times \sqrt{37})$ MoS$_2$. The corresponding strain of germanene is -5.4, -5.5, and -5.6%, respectively. The Fermi level is set to zero.

of germanene on top of a $(\sqrt{31} \times \sqrt{31})$ layer of MoS$_2$. Importantly, when looking at the DOS, as shown in Fig. 2(a), we can see that the Dirac cone of the supercell is placed at the Fermi level, as expected from the experimental results. Moreover, in Figs. 2(b) and 2(c) we show the charge density integrated from -0.3 to 0.0 eV and from 0.0 to 0.3 eV, respectively. As expected from the DOS, the charge is concentrated around the Ge atoms and does not show a modulation that would be due to the moiré pattern formed between germanene and MoS$_2$. This is in agreement with the scanning tunneling microscopy images found experimentally [12,13].

B. MoS$_2$ defects and charge puddles

In Sec. III A, we have seen that experimentally, when placing germanene on MoS$_2$ the latter does not suffer any kind of reconstruction and that, in order to describe correctly the electronic properties of the system, we need to generate supercells where germanene has its calculated free standing lattice constant (4.09 Å). In this section, we will shift our attention to the problem of charge puddles found in germanene on MoS$_2$ [13]. In order to investigate a possible doping of germanene, we consider several common defects that occur frequently in MoS$_2$.

As we have mentioned in the Introduction, MoS$_2$ samples fabricated by either CVD or exfoliation of geological samples may contain various defects and impurities [17,38]. Among CVD samples the most abundant and stable defects are S or Mo vacancies that come either from the chemical growth process or during the final exfoliation [19,38]. Other common imperfections of MoS$_2$ crystals include antisite defects where Mo (S) atoms take the place of S (Mo) atoms [38,39]. On the other hand, geological samples are characterized by a larger diversity of possible defects [17]. In addition to the aforementioned ones, natural samples are known to have impurities and substitutional atoms. The most abundant impurities typical to geological MoS$_2$ samples include Re, Zr, and Nb [17–20]. It is important to note that some of these impurities could be not detected by the standard techniques to check the purity of the sample (such as x-ray photoelectron spectroscopy). We have also taken into account those that are less abundant or that are detected by inferring from the experimental techniques, namely, Cl and P [19,21].

1. Substitutional defects

Substitutional defects are frequently found in experimental MoS$_2$ monolayer samples [19,38–40]. Theoretically, many different types of substitutional defects can be studied, but not all of them can be found or realized experimentally. Therefore, here, we only focus on the defect types which have been
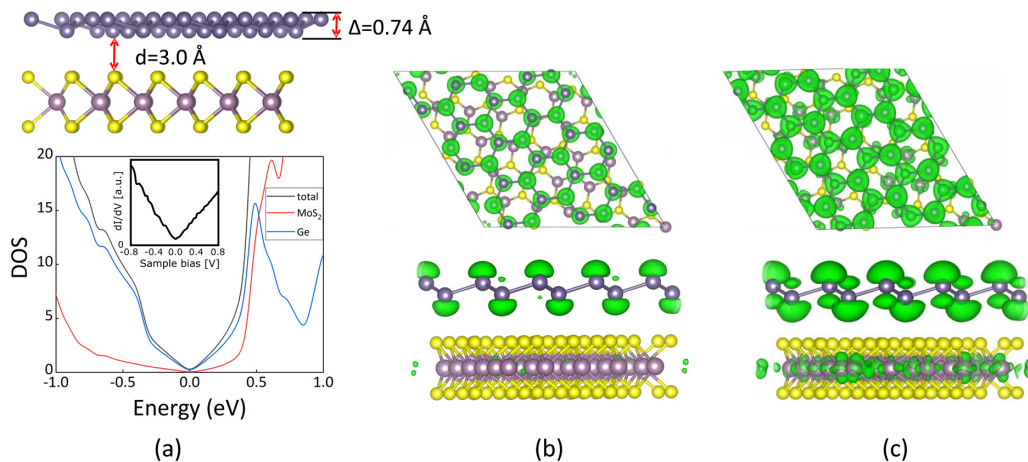

FIG. 2. (a) Top: Schematic diagram and structural parameters of a $(\sqrt{19} \times \sqrt{19})$ germanene layer on top of a $(\sqrt{31} \times \sqrt{31})$ MoS$_2$ layer with a twist angle of $14.5°$. Bottom: Calculated total and partial DOS of this structure. The Fermi level is set to zero. The inset shows the experimental dI/dV spectrum, adapted from the work by Zhang *et al.* [12]. (b), (c) Calculated partial charge density of the corresponding supercell in the energy range from -0.3 to 0.0 eV (b) and from 0.0 to 0.3 eV (c). The isosurface value is set to 2.5×10^{-4} e/Å^3. All the structures and density plots were visualized using VESTA [36].
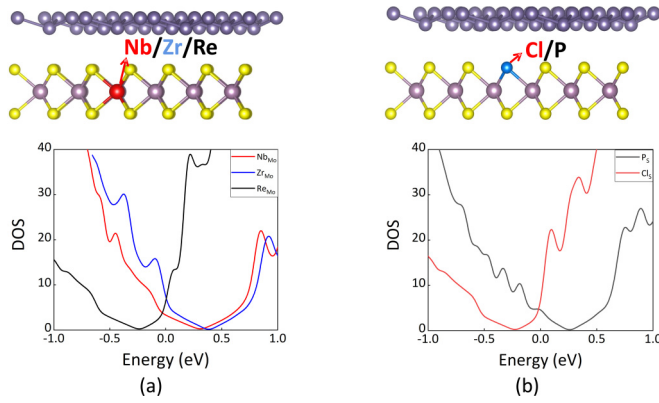
FIG. 3. Atomic structure of germanene on top of a defective MoS$_2$ layer (top row) and the corresponding total DOS (bottom row) of a (a) X_{Mo} system (X=Nb,Zr,Re) and (b) Y_S system (Y=Cl,P). The replaced atoms are highlighted in red and blue, respectively. The Fermi level is set to zero.

previously observed experimentally. Specifically, we consider the following situations.

a. The X atom (X = Nb,Zr,Re) replaces the Mo atom (X_{Mo}). As we have discussed before, niobium, zirconium, and rhenium are the most abundant impurities in geological MoS$_2$ samples. Furthermore, Re has been extensively studied since it is a common extrinsic dopant that can be easily introduced in experiments [17,20,40–42].

Here, without any loss of generality, we focus on a single atom substitution. In Fig. 3(a), we show the calculated DOS of a system doped with Nb, Zr, and Re atoms. Compared to the DOS of a pristine system, we can see that the Dirac cone shifts towards negative energies for the Re$_{Mo}$ system and to positive energies for the (Nb/Zr)$_{Mo}$ system, meaning that charge puddles can appear in samples with these defects in the MoS$_2$ layer. This is expected since the electron configuration of the Re/Nb/Zr and Mo are the same except for one (two) missing or one extra electron in the case of Nb (Zr) or Re, respectively. Interestingly, the MoS$_2$ defective system (without the germanene layer) has a very similar gap as the pristine case (see Fig. S6 in the SM [37]). In our case, we have a defect concentration of around 3.6×10^{13} cm^{-2}. This is comparable to the typical defect density reported previously (between 10^{12} and 10^{13} cm^{-2}) [38,43]. The calculated carrier concentrations are 3.3×10^{13}, 3.6×10^{13}, and 6.4×10^{13} cm^{-2} for the Re, Nb, and Zr substitutions, respectively. Accordingly, if we double the supercell size we have a defect concentration of 1.8×10^{13} cm^{-2} and the carrier concentration will be 1.7×10^{13} cm^{-2} (Re$_{Mo}$), 1.8×10^{13} cm^{-2} (Nb$_{Mo}$), and 3.2×10^{13} cm^{-2} (Zr$_{Mo}$) (see SM [37] for details). The partial charge density (see Fig. S5 in the SM [37]) for the Nb defect is slightly modified from the pristine case, but the charge in the germanene layer does not display a modulation, which is in agreement with previous experimental results [13].

b. The Y atom (Y = P,Cl) replaces the S atom (Y_S). Phosphorus-doped MoS$_2$ can be synthesized by a one-step hydrothermal method [44,45]. On the other hand, chlorine-doped MoS$_2$ systems have been studied both experimentally [46] and theoretically [47]. As in the case of Re/Nb/Zr substituting a Mo atom, P and Cl have the same

electronic configuration as S but with one missing and one extra electron, respectively. Figure 3(b) shows the calculated DOS, where a V-shaped Dirac cone is still present when S is replaced by Cl or P. For Cl, the Dirac point shifts to negative energy, indicating that the system is *p* doped, while if we substitute S with a P atom, we observe the shift towards positive energies, indicating that the system is *n* doped. This is expected from the electronic configurations. Here, as before, we only introduce one defect per supercell, which gives us a defect concentration of 3.6×10^{13} cm^{-2}. The calculated carrier concentrations (holes or electrons) are 3.7×10^{13} cm^{-2} and 3.1×10^{13} cm^{-2} for P and Cl, respectively. For the Cl defect, the system has a similar gap as the case without defects (see Fig. S6 in the SM [37]). As in the case with the Nb defect, the partial charge density (see Fig. S5 in the SM [37]) is slightly modified from the pristine case for the Cl defect, but the charge in the germanene layer does not display a modulation.

c. Other types of substitutional atoms. Finally, it has already been demonstrated that oxygen atoms can substitute sulfur atoms, forming stable MoS$_{2-x}$O$_x$ compounds both experimentally [48] and theoretically [49,50]. In our case, we investigate a single oxygen replacement. As it can be seen from the DOS calculation (see SM [37] for DOS results), the Dirac cone remains at the Fermi level, indicating that, for this kind of substitutions, there is no doping in the system. This is expected because the total number of electrons remains the same when we introduce the O$_S$ defect. There are other substitutional defects which have been investigated experimentally but, according to our calculations, they keep the system undoped, such as the case of a Se or Te atom substituting a S atom (Se$_S$, Te$_S$) and or sulfur adatom (S$_{ad}$) (see SM [37]).

In Fig. 4, we show the formation energies for all the defects considered in our paper. We can see that substitutional defects have a low formation energy which is in agreement with previous calculations [31].

The above results give a strong evidence that the doping defects in the substrate (MoS$_2$) layer can have an influence on the charge distribution of the germanene layer. It further demonstrates that different substitutional atoms present in natural MoS$_2$ samples can be responsible for some charge puddles appearing in the germanene layer as seen in the experiments by Yao *et al.* [13].

2. Sulfur vacancies

This type of defects has been predominantly seen in samples fabricated using mechanical exfoliation and CVD techniques [38]. Since these are common techniques used to fabricate the experimental devices, understanding the effect of these defects is important. Here, we generate a single sulfur vacancy (V_S) and a divacancy of sulfur atoms (V_{S2}) that are bonded to the same Mo atom. We have calculated the formation energy and found that a single S vacancy has the minimum formation energy of all vacancy defects, indicating it is the most stable and likely vacancy in MoS$_2$ (see Fig. 4). On the other hand, divacancies have a considerably higher formation energy, which makes them less likely to be seen in experimental samples. This is also the case for Mo vacancies (V_{Mo}). These results are in line with earlier theoretical cal-
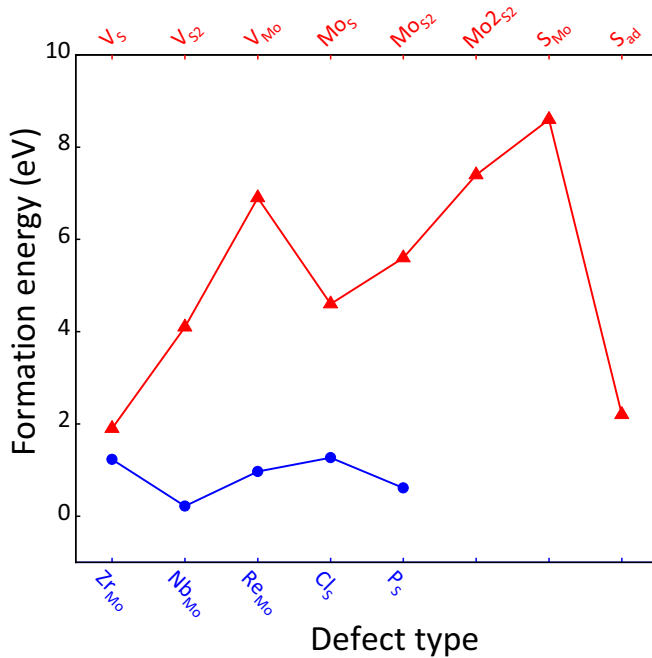
FIG. 4. Calculated formation energy (eV) of the different defects in MoS$_2$ considered in this paper. Substitutional defects are marked with blue circles while other types of defects are marked with red triangles.

culations [51], and experimental observations [38], reporting that sulfur deficiency is very common during the synthesis process. The structure and the calculated DOS for these systems are shown in Fig. 5. As we can see, near the Fermi level a peak in the DOS appears due to the defect and the characteristic V shape of the Dirac cone does not appear anymore in both systems. This peak is also found when looking at the MoS$_2$ defective supercell without the germanene layer (see Fig. S6 SM [37] for more details). It is clear then, that sulfur vacancies are unlikely to be responsible for the charge puddles found in the experiment. This is also in line with the partial charge density (see Fig. S5 in the SM [37]) obtained with this
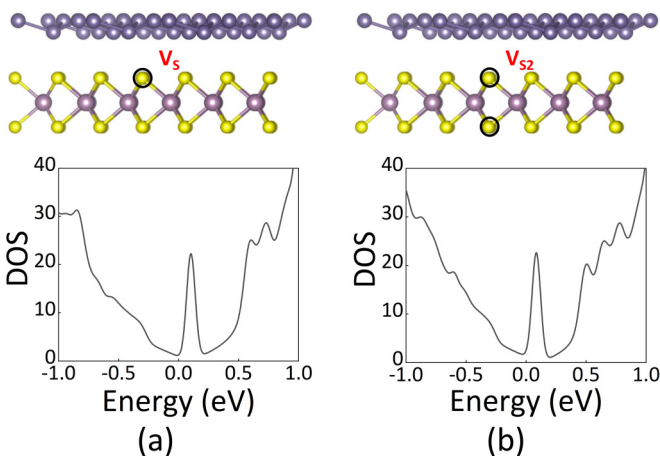

FIG. 5. Schematic diagram of germanene on MoS$_2$ substrate with sulfur vacancies, and the corresponding total DOS. (a) Single S vacancy. (b) S divacancy.
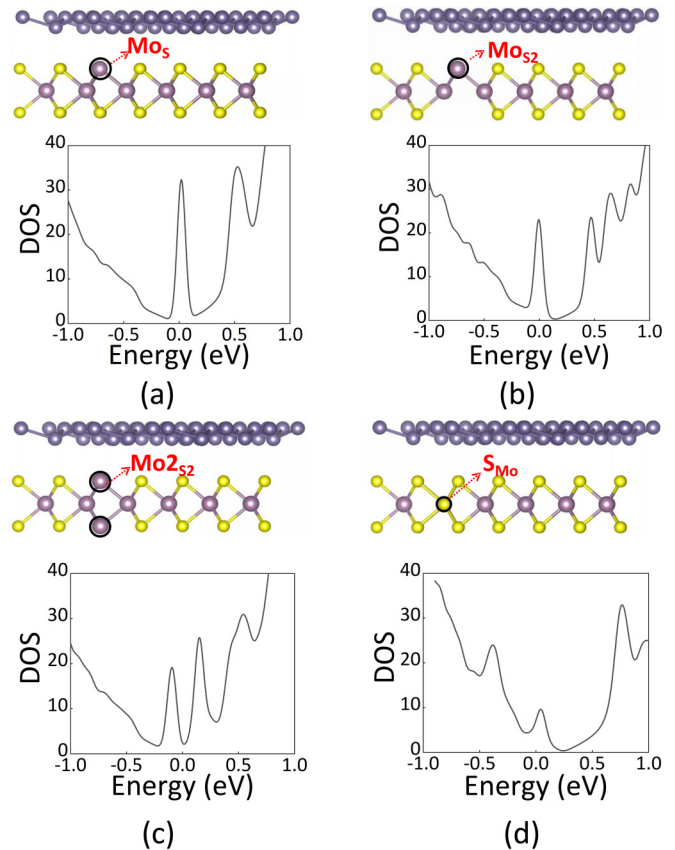

FIG. 6. Schematic diagram of germanene on MoS$_2$ with four kinds of the antisite defect, and their corresponding total DOS.

defect, which shows no charge concentrated around the Ge atoms.

3. Antisite defect

A thorough experimental study of antisite defects has been done by Hong *et al.* [38], where they observed five different types of antisite defects that can be classified in the following categories.

(i) One S atom is substituted by one Mo atom (Mo$_S$).

(ii) Two opposite S atoms are substituted by one Mo atom (MoS$_2$).

(iii) Two opposite S atoms are substituted by two Mo atoms (Mo2$_{S2}$).

(iv) One S atom takes the place of one Mo atom site (S$_{Mo}$).

(v) Two S atoms take the place of one Mo atom site (S2$_{Mo}$).

Since the last one is rarely found in experiments [38], we have studied the other four defect types mentioned above. The formation energies for these defects are shown in Fig. 4, where we can see that they have a higher formation energy than the single S vacancy and, therefore, are less likely to appear in real devices. In Fig. 6, we show the DOS for the different types of antisite defects. As in the case of the S vacancies, one or multiple peaks due to the defects appear in the DOS; midgap states appear in the gap of the defective MoS$_2$ layer without the germanene sitting on top (see Fig. S6 in the SM [37]). If the MoS$_2$ layer has one defect only, the peak sits at the Fermi

level while in the case of the MoS_2 defect the DOS displays two peaks near the Fermi level at negative and positive energies. Importantly, in all cases the Dirac cone is not preserved, indicating that these defect types are unlikely related to the charge puddles observed experimentally. As in the case with the sulfur vacancy, this result is also in line with the partial charge density (see SM [37]) obtained with the MoS defect, which shows no charge concentrated around the Ge atoms.

IV. CONCLUSIONS

In summary, using first-principles calculations, we have studied the electronic properties of germanene on top of a pristine and defective MoS_2 layer. We first studied the electronic structure of variety configurations changing the strain applied to the germanene layer. We found that minimization of the lattice mismatch between germanene and MoS_2 leads to the electronic structure with a prominent V shape where the Dirac cone is located exactly at the Fermi level, in agreement with the previous experimental results. Having properly aligned germanene and MoS_2, we further investigated the electronic properties in the presence of common point defects in the MoS_2 layer. From these results, we found that the charge puddles found in the germanene layer experimentally can likely be explained by substitutional defects in the MoS_2 substrate. Specifically, substitution of Mo by group IV-V and VII

transition metal atoms (Re, Nb, Zr) preserves the Dirac cone, but shifts the Fermi energy inducing the charge doping of germanene. Different types of doping (*n* doped and *p* doped) can be obtained by introducing different atoms, which might be present in natural MoS_2 samples. It is worth noting that a controllable introduction of these defects during the synthesis of MoS_2 opens up the possibility of tuning the position of the Dirac cone of germanene while leaving the electronic properties of the material unaltered. This mechanism might be useful in the realization of lateral *p-n* junctions based on 2D materials.

Our findings highlight the significance of the effect of the substrate even for weakly coupled van der Waals heterostructures and that the formation of charge puddles could be extended to other 2D Dirac materials supported on transition metal dichalcogenides.

ACKNOWLEDGMENTS

[1] S. Cahangirov, M. Topsakal, E. Aktürk, H. Şahin, and S. Ciraci, Phys. Rev. Lett. **102**, 236804 (2009).

[2] A. Acun, L. Zhang, P. Bampoulis, M. v. Farmanbar, A. van Houselt, A. Rudenko, M. Lingenfelder, G. Brocks, B. Poelsema, M. Katsnelson *et al.*, J. Phys.: Condens. Matter **27**, 443002 (2015).

[3] X.-S. Ye, Z.-G. Shao, H. Zhao, L. Yang, and C.-L. Wang, RSC Adv. **4**, 21216 (2014).

[4] M. E. Dávila, L. Xian, S. Cahangirov, A. Rubio, and G. L. Lay, New J. Phys. **16**, 095002 (2014).

[5] L. Li, S.-z. Lu, J. Pan, Z. Qin, Y.-q. Wang, Y. Wang, G.-y. Cao, S. Du, and H.-J. Gao, Adv. Mater. **26**, 4820 (2014).

[6] P. Bampoulis, L. Zhang, A. Safaei, R. van Gastel, B. Poelsema, and H. J. W. Zandvliet, J. Phys.: Condens. Matter **26**, 442001 (2014).

[7] M. Derivaz, D. Dentel, R. Stephan, M.-C. Hanf, A. Mehdaoui, P. Sonnet, and C. Pirri, Nano Lett. **15**, 2510 (2015).

[8] Q. Yao, L. Zhang, N. S. Kabanov, A. N. Rudenko, T. Arjmand, H. Rahimpour Soleimani, A. L. Klavsyuk, and H. J. W. Zandvliet, Appl. Phys. Lett. **112**, 171607 (2018).

[9] Q. Chen, L. Liang, G. Potsi, P. Wan, J. Lu, T. Giousis, E. Thomou, D. Gournis, P. Rudolf, and J. Ye, Nano Lett. **19**, 1520 (2019).

[10] B. Borca, C. Castenmiller, M. Tsvetanova, K. Sotthewes, A. N. Rudenko, and H. J. W. Zandvliet, 2D Mater. **7**, 035021 (2020).

[11] Z. Jiao, Q. Yao, A. N. Rudenko, L. Zhang, and H. J. W. Zandvliet, Phys. Rev. B **102**, 205419 (2020).

[12] L. Zhang, P. Bampoulis, A. N. Rudenko, Q. Yao, A. van Houselt, B. Poelsema, M. I. Katsnelson, and H. J. W. Zandvliet, Phys. Rev. Lett. **116**, 256804 (2016).

[13] Q. Yao, Z. Jiao, P. Bampoulis, L. Zhang, A. Rudenko, M. Katsnelson, and H. Zandvliet, Appl. Phys. Lett. **114**, 041601 (2019).

[14] W. Zhang, P. Zhang, Z. Su, and G. Wei, Nanoscale **7**, 18364 (2015).

[15] X. Li and H. Zhu, J. Materiomics **1**, 33 (2015).

[16] J. Sun, X. Li, W. Guo, M. Zhao, X. Fan, Y. Dong, C. Xu, J. Deng, and Y. Fu, Crystals **7**, 198 (2017).

[17] R. Addou, L. Colombo, and R. M. Wallace, ACS Nano **9**, 9124 (2015).

[18] F. D. Brandão, G. M. Ribeiro, P. H. Vaz, J. C. González, and K. Krambrock, J. Appl. Phys. **119**, 235701 (2016).

[19] R. Addou, L. Colombo, and R. M. Wallace, ACS Appl. Mater. Interfaces **7**, 11921 (2015).

[20] J. Golden, M. McMillan, R. T. Downs, G. Hystad, I. Goldstein, H. J. Stein, A. Zimmerman, D. A. Sverjensky, J. T. Armstrong, and R. M. Hazen, Earth Planet. Sci. Lett. **366**, 1 (2013).

[21] M. H. Whangbo, J. Ren, S. N. Magonov, H. Bengel, B. A. Parkinson, and A. Suna, Surf. Sci. **326**, 311 (1995).

[22] W. Kohn and L. J. Sham, Phys. Rev. **140**, A1133 (1965).

[23] J. M. Soler, E. Artacho, J. D. Gale, A. García, J. Junquera, P. Ordejón, and D. Sánchez-Portal, J. Phys.: Condens. Matter **14**, 2745 (2002).

[24] J. P. Perdew, K. Burke, and M. Ernzerhof, Phys. Rev. Lett. **77**, 3865 (1996).

[25] J. P. Perdew and Y. Wang, Phys. Rev. B **33**, 8800 (1986).

[26] N. Troullier and J. L. Martins, Phys. Rev. B **43**, 1993 (1991).

[27] S. Grimme, J. Comput. Chem. **25**, 1463 (2004).

[28] H. J. Monkhorst and J. D. Pack, Phys. Rev. B **13**, 5188 (1976).

[29] R. Cuadrado and J. I. Cerdá, J. Phys.: Condens. Matter **24**, 086005 (2012).

[30] S. B. Zhang and J. E. Northrup, Phys. Rev. Lett. **67**, 2339 (1991).

[31] A. Yoshimura, N. Koratkar, and V. Meunier, Nano Express **1**, 010008 (2020).

[32] J.-A. Yan, S.-P. Gao, R. Stein, and G. Coard, Phys. Rev. B **91**, 245403 (2015).

[33] Y. Wang and D. Yi, Solid State Commun. **155**, 6 (2013).

[34] M. Houssa, G. Pourtois, V. V. Afanas'ev, and A. Stesmans, Appl. Phys. Lett. **96**, 082111 (2010).

[35] N. J. Roome and J. D. Carey, ACS Appl. Mater. Interfaces **6**, 7743 (2014).

[36] K. Momma and F. Izumi, J. Appl. Crystallogr. **44**, 1272 (2011).

[37] See Supplemental Material at http://link.aps.org/supplemental/10.1103/PhysRevB.105.094111 for the results of the calculated DOS of other structures, including germanene on pristine and defective MoS_2, the details for the estimation of the carrier concentration, the partial charge distribution, and the study of the band gap in the defective systems.

[38] J. Hong, Z. Hu, M. Probert, K. Li, D. Lv, X. Yang, L. Gu, N. Mao, Q. Feng, and L. Xie, Nat. Commun. **6**, 6293 (2015).

[39] J.-Y. Tsai, J. Pan, H. Lin, A. Bansil, and Q. Yan, Nat. Commun. **13**, 492 (2022).

[40] S. Kim, J. Lim, R. Sahu, O. Kasian, and B. Gault, Adv. Mater. **32**, 1907235 (2020).

[41] K.-K. Tiong, P. Liao, C. Ho, and Y. Huang, J. Cryst. Growth **205**, 543 (1999).

[42] T. Hallam, S. Monaghan, F. Gity, L. Ansari, M. Schmidt, C. Downing, C. P. Cullen, V. Nicolosi, P. K. Hurley, and G. S. Duesberg, Appl. Phys. Lett. **111**, 203101 (2017).

[43] D. Chiappe, I. Asselberghs, S. Sutar, S. Iacovo, V. Afanas'ev, A. Stesmans, Y. Balaji, L. Peters, M. Heyne, M. Mannarino, W. Vandervorst, S. Sayan, C. Huyghebaert, M. Caymax, M. Heyns, S. De Gendt, I. Radu, and A. Thean, Adv. Mater. Interfaces **3**, 1500635 (2016).

[44] J. S. Lee, C.-S. Park, T. Y. Kim, Y. S. Kim, and E. K. Kim, Nanomaterials **9**, 1278 (2019).

[45] X. Xin, Y. Song, S. Guo, Y. Zhang, B. Wang, Y. Wang, and X. Li, J. Alloys Compd. **829**, 154635 (2020).

[46] T. Kim, Y. Kim, and E. K. Kim, Sensors and Actuators A: Physical **312**, 112165 (2020).

[47] H. Zou, Q. Zeng, M. Peng, W. Zhou, X. Dai, and F. Ouyang, Solid State Commun. **280**, 6 (2018).

[48] Z. Wei, J. Tang, X. Li, Z. Chi, Y. Wang, Q. Wang, B. Han, N. Li, B. Huang, J. Li *et al.*, Small Methods **5**, 2100091 (2021).

[49] L.-J. Kong, G.-H. Liu, and L. Qiang, Comput. Mater. Sci. **111**, 416 (2016).

[50] A. V. Krivosheeva, V. L. Shaposhnikov, V. E. Borisenko, J.-L. Lazzari, C. Waileong, J. Gusakova, and B. K. Tay, J. Semicond. **36**, 122002 (2015).

[51] K. Santosh, R. C. Longo, R. Addou, R. M. Wallace, and K. Cho, Nanotechnology **25**, 37 (2014).